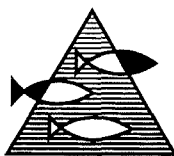


PROSJEKTRAPPORT

ISSN 0071-5638



HAVFORSKNINGSINSTITUTTET

MILJØ - RESSURS - HAVBRUK

Nordnesparken 2 Postboks 1870 5024 Bergen

Tlf.: 55 23 85 00 Faks: 55 23 85 31

Forskningsstasjonen

Flødevigen
4817 His

Tlf.: 37 05 90 00

Faks: 37 05 90 01

Austevoll

Havbruksstasjon
5392 Storebø

Tlf.: 56 18 03 42

Faks: 56 18 03 98

Matre

Havbruksstasjon
5198 Matredal

Tlf.: 56 36 60 40

Faks: 56 36 61 43

Distribusjon:

ÅPEN

HI-prosjektnr.:

02.01.03

Oppdragsgiver(e):

EU-MAST project

Oppdragsgivers referanse:

MAS3-CT-0070

Rapport:

FISKEN OG HAVET

NR. 3 - 1999

Tittel:

EFFECTS OF INSUFFICIENT VERTICAL
RESOLUTION IN A 3D COASTAL OCEAN MODEL

Sender:

Marine environment

Seksjon:

Physical oceanography

Forfatter(e):

Lars Asplin

Antall sider, vedlegg inkl.:

19

Dato:

28.02.1999

Sammendrag:

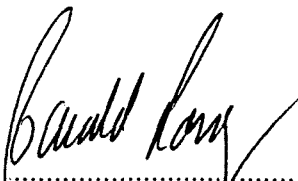
The consequences of not resolving vertical gradients (of velocity or density) in a three-dimensional numerical model are investigated. The results show that the effects of insufficient vertical resolution are significant and can be difficult to discover in complex numerical simulations. Calculations of the vertical wind-driven velocity of the Ekman layer need fine resolution in the upper few meters to avoid an underestimation of the surface velocity and a small overestimation of the velocity below 5-10 m depth. Calculations of upper brackish-layer flow show that an insufficient vertical resolution leads to quantitative large errors, but in the present experiment, the qualitative errors are modest. Especially in connection with applications involving water quality models and biological models, the errors induced by insufficient vertical resolution can be critical.

Emneord - norsk:

1. Numerisk havmodellering
2. Blandingslag
3. Overflatestrøm

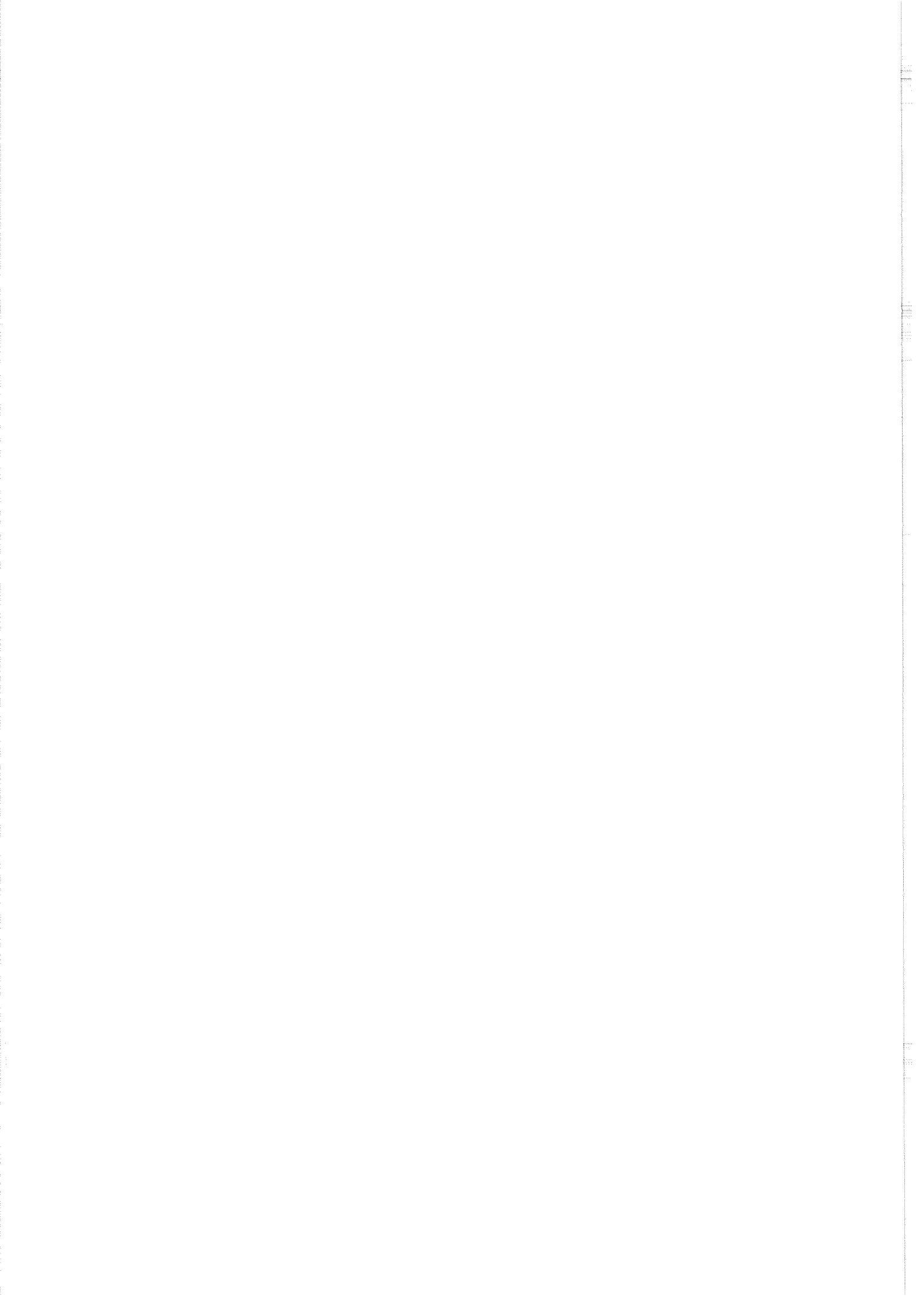
Emneord - engelsk:

1. Numerical simulations
2. Surface mixed layer
3. Surface current


.....
Prosjektleder


.....
Seksjonsleder

R 5957



Effects of insufficient vertical resolution in a 3D coastal ocean model

Lars Asplin

Institute of Marine Research
Nordnesgaten 50, Postbox 1870 Nordnes
N 5024 Bergen, Norway

February, 1999

1. Introduction

The dynamics of the coastal ocean are characterized by many different horizontal and vertical scales due to its complicated forcing, stratification, and topography. To make proper numerical simulations of coastal ocean dynamics, the numerical grid must resolve the important length scales with several grid-points (the sampling theorem indicates a minimum of two, a rule-of-thumb says ten). Thus, in the vicinity of the coast and inside estuaries and fjords, a preferable horizontal grid resolution is 10-100 m and vertical resolution less than 1 m. Such a fine resolution is impossible with the present computer resources if reasonable geographical areas are to be covered. As a compromise, it is often necessary to use a coarser grid as long as the effects of this can be parameterized.

In the vertical, several typical length scales exist, many of which are quite short ($O(1\text{ m})$ - $O(10\text{ m})$). Bottom boundary layers (due to tidal currents) and surface mixed layers (due to e.g. winds) are common. Baroclinic coastal currents can have a complicated vertical structure, and coastal upwelling and downwelling are common phenomena further complicating the vertical structure of coastal waters. In estuaries and fjords, freshwater runoff creates brackish plumes flowing in shallow (1-5 m deep) surface layers. Clearly, to resolve all such vertical scales one needs fine resolution from surface to bottom.

The present work is an investigation of some consequences connected with insufficient vertical resolution in 3D numerical modelling. Two typical physical oceanographical features common in coastal waters are studied: Wind-driven flow (homogeneous water for simplicity), and surface brackish-layer flow due to river runoff. Both these phenomena have strong sub-surface gradients and are characterized by vertical scales of only a few metres, thus both are naturally demanding regarding vertical resolution in numerical models. The experiments are idealized in order to easily verify the results of the numerical simulations, and are arranged as a comparison study where only the vertical grid resolution will differ from simulation to simulation. A control simulation with sufficient vertical resolution will represent the "true solution" given by the model (although this might of course be erroneous compared to nature due to other limitations of the numerical model). The results of simulations with less vertical sampling rate will be compared to the results of the control simulation.

The paper is organized as follows: Section 2 gives a description of the numerical model used for the study, section 3 presents the simulations and results for the wind driven flow, section 4 presents the simulations and results for the brackish-layer flow, and finally, section 5 concludes the work.

2. The numerical model

The numerical model used for the simulations is the so-called Ecom3d [Blumberg and Mellor, 1987]. Another version of this model is the widely used Princeton Ocean Model, [Mellor, 1996]. Ecom3d is a three-dimensional, primitive equation, time-dependent, σ -coordinate, free surface estuarine and coastal ocean circulation model. The model is designed to address phenomena of 1-100 km length scale and tidal to monthly time scale. It

can be used with an orthogonal curvilinear grid, but for the present a rectangular uniform grid is used. One of the advantages of Ecom3d is its embedded turbulence closure submodel [Mellor and Yamada, 1982]. The prognostic variables are three components of velocity, potential temperature, salinity, surface elevation and two variables representing turbulent length scale and turbulent kinetic energy. The model uses the hydrostatic assumption and the Boussinesq approximation. The governing equations are the equations for conservation of mass, momentum, temperature and salinity along with the hydrostatic equation in the vertical and an equation of state relating salinity and potential temperature to potential density. The equations are solved by finite difference techniques on a staggered Arakawa C-grid. The horizontal time differencing is explicit whereas the vertical differencing is implicit. The latter eliminates time constraints for the vertical coordinate and permits the use of fine vertical resolution in e.g. the surface and bottom boundary layers. A split time step is used in the model: an external mode portion calculated by a two-dimensional set of equations with a short time step based on the CFL condition and the external wave speed, and an internal mode calculating the full three-dimensional equations at a longer time step based on the CFL condition and the internal wave speed.

Ecom3d uses a leap-frog numerical advection scheme for horizontal fluxes. Due to numerical dispersion errors (over and under shooting) this advection scheme can perform poorly in regions of large gradients, e.g. when simulating freshwater runoff. To prevent these numerical dispersion errors, a new advection scheme for salt and temperature replacing the leap-frog has been implemented: A total variation diminishing (TVD) flux limiter advection scheme using a superbee limiter due to Roe and Sweby [Sweby, 1984]. The scheme is 2nd order accurate in areas with small gradients, gradient preserving near fronts, and monotonic (especially important in water-quality applications).

Originally, Ecom3d is implemented with a vertical boundary condition making the turbulent length scale zero at the surface. This, obviously, is an underestimation of reality. Hence, the present code is modified as suggested by Melsom [1996] with the following vertical boundary condition (at the depth Z below the surface corresponding to the level of the $\sigma(2)$ surface):

$$Q2L = \kappa ZQ2 ,$$

where $Q2L$ is the model variable representing turbulent length scale, $Q2$ is the variable representing twice the turbulent kinetic energy, and κ is the von Kármán's constant ($\kappa = 0.4$).

Since the introduction in the late seventies, Ecom3d and the Princeton Ocean Model have become widely used by researchers all over the world. Currently, 249 users from 33 different countries are registered users. Reports of the model performance are numerous, and references to published papers can be found electronically at the home page of the Princeton Ocean Model (URL: <http://www.aos.princeton.edu/WWWPUBLIC/htdocs.pom/>).

3. Wind-driven flow

The basic theory for wind-driven flow was given by Ekman [1905] including the robust result that the volume flux is directed 90° to the right of the wind (northern hemisphere) with its magnitude independent of the vertical distribution of velocity. This result is probably why most numerical ocean models calculate tides and volume fluxes reasonably well, and observations also to a great extent support the Ekman theory for the volume flux [e.g. Stacey *et al.*, 1986; Price *et al.*, 1986; Lentz, 1992; Chereskin, 1995; Weller and Plueddemann, 1996]. As to the vertical profile of the wind-driven flow, it is widely agreed that the theory predicted by Ekman is too simple. Crucial in the determination of the vertical profile of the velocity is the turbulent mixing, a phenomenon yet to be fully described. Recent theory [Craig and Banner, 1994] assumes that the horizontal velocity below the ocean surface has a logarithmic vertical profile analogous to the “wall theory”. Observations of the wind-driven velocity profile are characterized by an extremely low signal-to-noise ratio, however, most reported observations find a velocity shear in the vertical as a statistical mean [Stacey *et al.*, 1986; Lentz, 1992; Krauss, 1993; Chereskin, 1995; Gnanadesikan and Weller, 1995; Weller and Plueddemann, 1996]. Scalar quantities such as temperature and salinity, on the other hand, are usually homogeneous in the mixed layer. In Ecom3d the turbulent mixing coefficients are calculated by the embedded turbulent closure model of Mellor and Yamada [1982]. Craig and Banner [1994] show that this closure model gives reasonable results for the vertical velocity profile, although, as long as the closure model operates inside a coarse gridded ocean model, several small-scale dynamical features that could have been handled (through the exchange of the 3D velocity from the ocean model) will not be included. In particular these are the effects of breaking waves [e.g. Craig, 1996] and wave-current interaction or Langmuir circulation [Gnanadesikan and Weller, 1995; Skillingstad and Denbo, 1995].

The present investigation considers an idealized experiment (most of Ekman’s [1905] assumptions), and uses the full 3D model although the problem is of a one-dimensional nature (variations only in the vertical). The model domain consists of a 810 km by 810 km rectangular homogeneous coastal ocean with a flat bottom of 50 m depth. Note that with a flat bottom, the vertical σ -coordinate system is similar to a z-coordinate system (except for small vertical displacement of the σ -levels in accordance with surface elevations). In the middle of the domain is a 200 km by 200 km wind field with a constant wind stress $\tau = 0.1 \text{ N/m}^2$ in positive x-direction. The initial conditions are: no motion, no surface elevation, salinity of 33, and a temperature of 10°C . Along the boundaries, the so-called FRS open boundary condition (flow relaxation scheme, Martinsen and Engedahl [1987]) is applied. The horizontal numerical grid has an equidistant grid size of 10 km in both x and y directions. The vertical grid (staggered, with the horizontal velocity calculated midway between the σ -levels) vary from one simulation to the other, while the other variables or conditions are equal for all simulations. Ten simulations were performed, of which six simulations with equidistant grid: *dz1* (51 σ -levels; $\Delta z = 1$ m), *dz2* (26 σ -levels; $\Delta z = 2$ m), *dz3* (18 σ -levels; $\Delta z = 3$ m), *dz5* (11 σ -levels; $\Delta z = 5$ m), *dz10* (6 σ -levels; $\Delta z = 10$ m), and *dz15* (5 σ -levels; $\Delta z = 15$ m). Four simulations have variable vertical grid spacing: *vrbl* (19 σ -levels; 0, 0.5, 1, 1.5, 2, 3, 4, 5, 6, 8, 10, 12.5, 15, 20, 25, 30, 40, 45, and 50 m), *vrb2* (52 σ -levels; 0-2 m: $\Delta z = 0.2$ m, 2-10 m: $\Delta z = 0.5$ m, 10-20 m: $\Delta z = 1$ m, 20-50 m: $\Delta z = 2$ m), *vrb3* (8 σ -levels; 0, 1, 5, 10, 20, 30, 40, and 50 m), and *vrb4* (10 σ -levels; 0, 0.5, 1, 10, 20, 30, 40, 44, 48, and 50 m).

For the many different parameter settings of Ecom3d (Mellor [1996]), the following applies to all ten simulations: The internal time-step (3D equations) is 900 s, and the external time-step is 150 s (the CFL-criterion is 159 s). The total simulation time is 168 hours. The Coriolis parameter is constant and equal to $1.37 \cdot 10^{-4} \text{ s}^{-1}$. The parameter of the horizontal diffusion term (Smagorinsky [1963]) is 0.1 (HORCON or C). The minimum value of the coefficient for turbulent viscosity is $2.5 \cdot 10^{-5} \text{ m}^3/\text{s}$ (UMOL), while the minimum value for the turbulent diffusivity of salt and temperature is $10^{-7} \text{ m}^3/\text{s}$ (UMOLPR). The parameter of the Asselin time-filter is 0.1 (SMOTH or α).

The wind forcing takes place in the middle of the model domain (far away from the open boundaries), and the results will include a component of geostrophically balanced flow in the downwind direction due to sea-surface elevation gradients. Although this wind field is somewhat unrealistic, the experiment serves well as a comparison study. The results will be presented at the grid box (40,40) in the middle of the wind-forced area after 168 simulated hours. Values of volume flux calculated from the depth-averaged velocities in and out of the horizontal grid box and the vertical profile of the horizontal velocity will be shown.

Table 1 lists the values of volume flux in the along-wind direction (Q_x), the across-wind direction (Q_y), the assumed geostrophic-flow component ($U(30 \text{ m})$, the downwind horizontal velocity at 30 m depth), the along-wind volume flux with the geostrophic part subtracted (Q_x^{wind}), and the calculated angle (ϕ) between the wind direction and the volume flux vector due to the wind. Note the relatively large geostrophic part of the volume flux (Krauss [1993] pointed out that pressure driven flow components often totally dominates over wind-driven components in the surface mixed layer). If one assumes that the cross-wind component is a representative indication of the wind-driven portion of the total flow, one finds that six of the ten simulations (*vrbl*, *vrb2*, *vrb4*, *dz1*, *dz2*, and *dz3*) deviate by maximum 4%. Using the mean value of these six simulations, the other four simulations relate as this: *dz5*, 93%; *vrb3*, 84%; *dz10*, 71%; *dz15*, 68%. Obviously, with a coarser grid, a smaller part of the wind-driven flow is captured. Looking at the assumed geostrophic-flow component ($U(30 \text{ m})$), however, all simulations have values within 1 cm/s.

Table 1: Results of the wind-driven flow experiments

Simulation	Q_x [m ³ /s]	Q_y Table 2: [m ³ /s]	U(30 m) [m/s]	Q_x^{wind} [m ³ /s]	ϕ [°]
vrbl	66410	-7350	0.129	1910	75
vrb2	66330	-7680	0.129	1830	77
vrb3	68160	-6370	0.130	3160	64
vrb4	67640	-7630	0.132	1640	78
dz1	67570	-7660	0.132	1570	78
dz2	66410	-7590	0.130	1410	80
dz3	66910	-7510	0.131	1410	79
dz5	66370	-7050	0.129	1870	75
dz10	68900	-5340	0.132	2900	62
dz15	70260	-5120	0.138	1260	76

Table 1. The values of volume flux after 168 hours at the grid box (40,40) in the middle of the wind-forced area for the ten simulations of the wind-driven flow experiment. Q_x and Q_y are the volume flux in the along-wind and across-wind directions respectively. $U(30\text{ m})$ is an estimation of the geostrophic current, and Q_x^{wind} is the net along-wind volume flux after subtraction of the geostrophic part. ϕ is the angle between the wind vector (positive x-direction) and the volume flux vector (Q_x^{wind}, Q_y).

A more demanding task for the numerical model is to calculate the vertical profile (shear) of the horizontal velocity. Figure 1 presents these profiles at the grid cell (40,40) after 168 hours for the six simulations with equidistant vertical grid, shown as the u -component (parallel to the wind) and the v -component in separate curves. The vertical extension of the wind-driven flow (the Ekman layer) can be taken roughly to be 20 m. A commonly used expression for calculation of the mixed layer depth is:

$$h \approx \kappa \frac{u_*}{f},$$

where u_* is the friction velocity, f is the Coriolis parameter, and κ often is taken to be the von Kármán's constant ($\kappa = 0.4$). Using this expression we get $h = 29\text{ m}$ ($f = 1.37 \cdot 10^{-4}\text{ s}^{-1}$, $u_* = \sqrt{\tau/\rho} = 0.01\text{ m/s}$), somewhat larger than the values from the numerical simulations. There may be two reasons for this: 1. Stigebrandt [1985] found from a series of observations that the factor 0.4 in the above expression for the mixed layer depth was too high. He got a better fit when using the value 0.2, and in our case this yields a mixed layer depth of about

15 m. 2. Martin [1985] found that the turbulence closure scheme used in the numerical model underpredicts mixed layer depth (although without the surface boundary condition for turbulent length scale as suggested by Melsom [1996]).

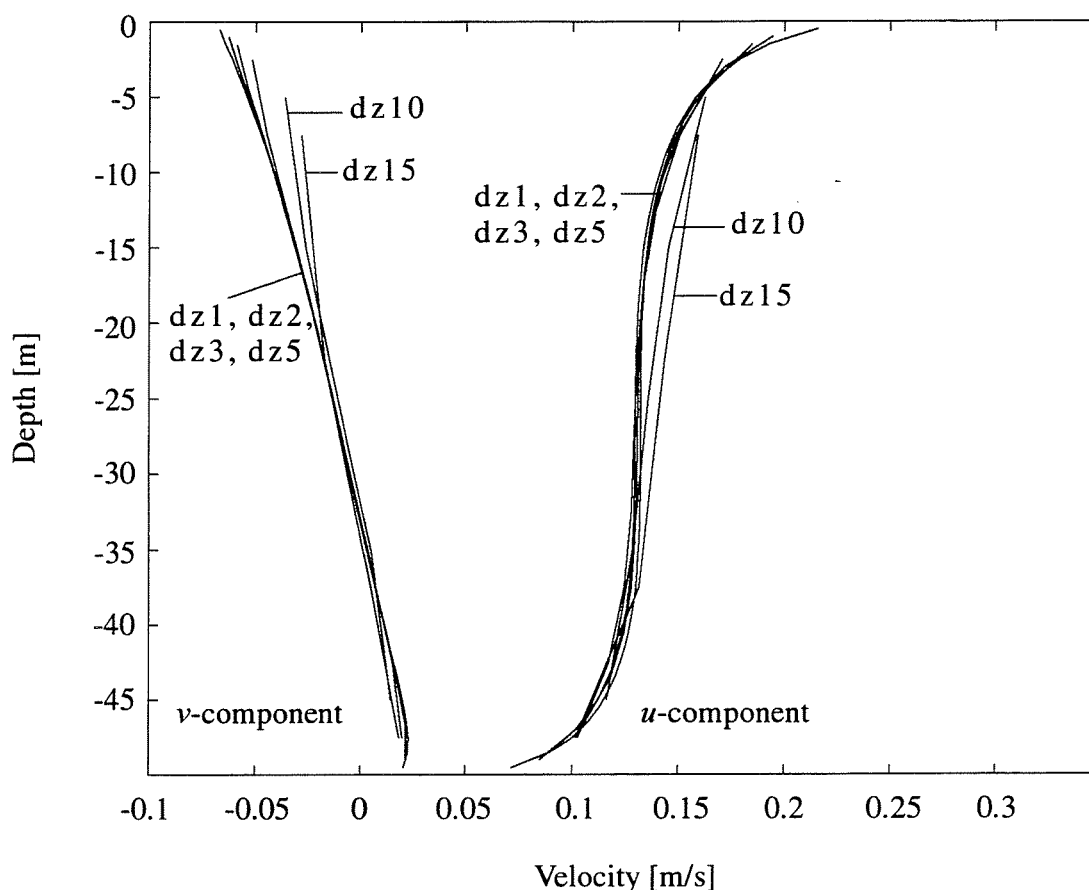


Figure 1. Vertical profiles of the horizontal velocity from the wind-driven flow experiments with equidistant vertical grid spacing. The u component is parallel to the wind direction while the v component is perpendicular. The bottom depth is 50 m.

Back to the vertical profiles of velocity, it is clear from Figure 1 that all simulations $dz1$, $dz2$, $dz3$, and to some degree $dz5$ follow the same profile. For the simulations $dz10$ and $dz15$, none of them capture the logarithmic velocity profile of the wind-driven part of the flow. Instead, compared to the simulations $dz1-dz5$, the flow is exaggerated. Since the vertical grid is staggered, with the calculation of horizontal velocities midway between the σ -levels, information of the near surface velocity is lost when the grid size increases. The uppermost level for calculation of the horizontal velocity components is for simulation $dz1$ 0.5 m, for simulation $dz2$ 1 m, for simulation $dz3$ 1.5 m etc. Looking at the magnitudes of the horizontal velocity vector in the upper grid cell (often interpreted as representative of the true surface velocity vector), it becomes less as the resolution decreases. For instance, the “surface velocity” of simulation $dz1$, located at 0.5 m depth, has a magnitude of 0.22 m/s, while in

contrast, the “surface velocity” of simulation *dz5* is located at 2.5 m depth and has a magnitude of 0.18 m/s. These results are in agreement with the findings of Blumberg and Mellor [1983] that briefly investigated a similar problem in a numerical study of the circulation of the South Atlantic Bight.

Figure 2 presents the vertical profiles of horizontal velocity from the simulations *vrbl-4* in the same manner as Figure 1. An obvious problem with an equidistant grid is that the real surface flow will not be calculated unless one uses a large number of grid nodes. With a nonuniform grid this is avoided as one can employ more grid nodes where needed (the variations are large). This is clearly seen by the smooth vertical profiles of the simulations *vrbl* and *vrb2*. The *vrb2* simulation has the finest vertical grid and is supposed to give the most exact results, while the simulation *vrbl* is assumed to have the most practical (cost efficient) vertical grid. Thus, it is reassuring to find that the vertical profiles from simulations *vrbl* and *vrb2* are almost identical, although due to the strong sub-surface velocity gradient the magnitude of the horizontal velocity vectors of the upper grid cell are for simulation *vrbl* 0.24 m/s (at 0.25 m depth) and 0.27 m/s for simulation *vrb2* (at 0.10 m depth). For the simulation with the coarser grid, *vrb3*, the results follow the tendency of the simulations *dz10* and *dz15* to slightly overestimate the velocity compared to the other simulations, and the wind-driven portion of the flow is only partly captured (although better than for the simulations *dz10* and *dz15*). Simulation *vrb4* has three σ levels in the upper metre and a grid distance between σ -level 3 and σ level 4 stretched by a factor 18 compared to the distance between σ -level 2 and σ -level 3. Apparently from Figure 2, the vertical profile of simulation *vrb4* is comparable to those of simulations *vrbl* and *vrb2* below 5 m depth, but with the near surface values being much exaggerated (simulation *vrb4*: 0.32 m/s, simulation *vrbl*: 0.24 m/s, both at 0.25 m depth).

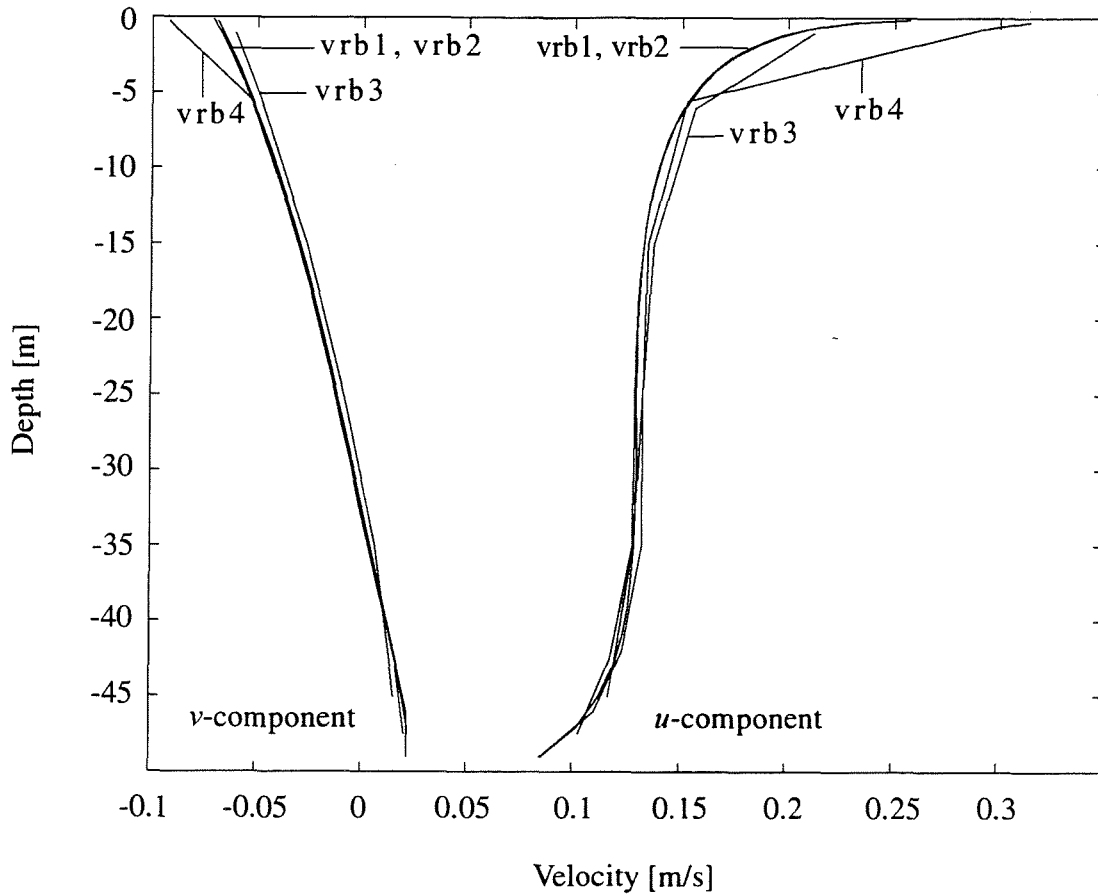


Figure 2. Vertical profiles of horizontal velocity from the wind-driven flow experiments with variable vertical grid spacing. The u component is parallel to the wind direction while the v component is perpendicular. The bottom depth is 50 m.

The exaggerated near surface velocity of simulation *vrbl* needs a closer examination. One obvious candidate responsible for this result is the truncation error of the finite difference scheme. However, truncation errors due to nonuniform grids are reported to be small [Treguier *et al.*, 1996]. Another possible explanation for the velocity increase is that the vertical dynamics are not resolved by the grid, and an aliasing of the unresolved energy appears. A simple one-dimensional, one component model of the diffusion equation ($\frac{\partial u}{\partial t} = KM \frac{\partial^2 u}{\partial z^2}$) will be used for this examination. The equation is discretized on a finite difference grid similar to that of Ecom3d (Equation 9-1, Mellor [1996]). The following discretized equation appears when the terms of $O(\Delta z^2)$ are included:

$$u_k^{n+1} - u_k^{n-1} = \frac{2\Delta t}{D^2 DZ_k^n} \left[\frac{KM_k^n}{DZZ_{k-1}^n} (u_{k-1}^n - u_k^n) - \frac{KM_{k+1}^n}{DZZ_k^n} (u_k^n - u_{k+1}^n) + R_{k+1}^n - R_k^n \right].$$

Here, k denotes the σ -level ($k = 1$ for the surface), n is the time level, Δt is the time step, D

is the bottom depth, Z_k is the relative depth of σ -level k ($Z_k * D$ is the depth in metres), DZ_k is the distance between the σ -levels Z_k and Z_{k+1} , DZZ_k is the distance between the levels where horizontal velocities are calculated (midway between the σ -levels), KM is the turbulent viscosity coefficient, and u is the velocity component parallel to the surface forcing vector (determined by the boundary condition for the stress at the surface, Z_1). R is the term of $O(\Delta z^2)$ from the differencing procedure and is expressed

$$R_k = \frac{1}{4} u''(Z_k) KM_k (DZ_{k-1} - DZ_k).$$

The term $u''(Z_k)$ is the second derivative of u at the depth Z_k .

Six simulations with different vertical grids were performed. Common for all simulations were the positions of the upper three σ -nodes: 0, 0.5, and 1 m. Below 1 m the grid distance is stretched compared to the 0.5 m above, and the following stretch factors were used: 2 (simulation *S2*, vertical grid similar to the vertical grid of the 3D simulation *vrbl*), 3 (simulation *S3*), 4 (simulation *S4*), 18 (simulation *S18*, similar to the vertical grid of the 3D simulation *vrbl4*), and 28 (simulation *S28*). In addition, a control simulation with a uniform high-resolution grid ($\Delta z = 0.05$ m) was performed. The bottom depth is 50 m and the stress used for surface boundary condition is as in the 3D simulation (0.1 N/m^2). For simplicity, the vertical viscosity coefficient (KM) is constant. Results after 1 simulated hour will be presented. The value of $u''(Z_k)$ is estimated from an exponential profile of u .

The important results from the different simulations are gathered in Table 2. Column 2 and 3 of Table 2 list the calculated velocities u and uR at 0.25 m depth with a constant turbulent viscosity coefficient $KM = 10^{-3} \text{ m}^2/\text{s}$. The velocity u is calculated without the terms of $O(\Delta z^2)$ while these are included in the calculation of uR . The differences between u and uR will then be an approximation to the truncation errors of $O(\Delta z^2)$. A quick examination of the numbers in Table 2 discovers that these errors are negligible, and that an increase of surface velocity appears as the vertical grid is stretched, independent of the terms of $O(\Delta z^2)$. This supports the findings of Treguier *et al.* [1996] stating that truncation errors are negligible in a vertically stretched grid. Hence, there must be another reason for the observed increase of velocity. Changing the turbulent viscosity coefficient to $KM = 10^{-1} \text{ m}^2/\text{s}$, the surface stress will be distributed deeper and the velocity profile will be smoother (i.e. longer wavelengths). Such a velocity profile, although probably unrealistic, is properly resolved by less vertical nodes. Column 4 of Table 2 shows that the differences between the results of the simulations with different grid stretching now are modest. While the velocity of simulation *S18* for $KM = 10^{-3} \text{ m}^2/\text{s}$ is 48% larger than that of *S2*, the difference is less than 1% when $KM = 10^{-1} \text{ m}^2/\text{s}$. Illustrated in Figure 3 are the vertical profiles of u for simulations *S2* and *S18* for both values of KM . Due to the strong vertical gradient in the upper 10 metres when $KM = 10^{-3} \text{ m}^2/\text{s}$, the increased velocity from the grid stretching is most likely due to aliasing of the unresolved dynamics.

Table 2: Results of the experiments with the 1D model

Simulation	KM=10 ⁻³ [m ² /s]		KM=10 ⁻¹ [m ² /s]	
	u(0.25 m) [m/s]	uR(0.25 m) [m/s]	u(0.25 m) [m/s]	uR(0.25 m) [m/s]
control	0.1900	0.1900	0.0212	0.0212
S2	0.1903	0.1902	0.0214	0.0213
S3	0.1954	0.1951	0.0214	0.0213
S4	0.2019	0.2013	0.0214	0.0213
S18	0.2816	0.2808	0.0215	0.0211
S28	0.3072	0.3066	0.0220	0.0212

Table 2. Values of velocities at 0.25 m depth for the results of the experiments with the one-dimensional diffusion-equation model. The velocities u and uR have truncation errors of $O(\Delta z^2)$ and $O(\Delta z^3)$ respectively.

The depth averaged kinetic energy can be calculated as $E_k = 0.5\rho \overline{v^2}$ (\overline{v} is the vertical mean velocity). Using $\rho = 1025 \text{ kg/m}^3$, the kinetic energy relative to that of the control simulation is for simulations $S2$, $S3$, $S4$, $S18$, and $S28$ respectively: $E_{k2} = 1.00$, $E_{k3} = 1.14$, $E_{k4} = 1.29$, $E_{k18} = 5.88$, $E_{k28} = 13.05$. Hence, a rather dramatic increase of energy appears as the grid is stretched in this particular situation. However, if a geostrophic background current is included, this energy increase will be masked. For instance, adding a geostrophic component of 0.13 m/s gives the following depth averaged kinetic energies (relative to that of the control simulation): $E_{kg2} = 1.00$, $E_{kg3} = 1.00$, $E_{kg4} = 1.00$, $E_{kg18} = 1.02$, $E_{kg28} = 1.05$.

4. Brackish-layer flow

In this section the level of complication is raised compared to the simulations of the previous section as the vertical resolution of a density profile is added to the problem. Hence, not only kinetic energy is involved but also the potential energy. Brackish-layer flow is chosen for this investigation of insufficient vertical resolution since it represents a clear-cut phenomenon easily identified.

A typical brackish layer from a freshwater runoff extends only a few metres down from the surface, and there is usually a sharp pycnocline at the base [Garvine, 1974, 1986; Garvine and Monk, 1974; Asplin, 1994a; Asplin *et al.*, 1995; Kaartvedt and Svendsen, 1995]. When the river meets the sea, the freshwater will mix with the saline sea water and form a brackish

intrusion. As the intrusion penetrates seawards, mixing with the surrounding water diminishes and eventually stops if no external mixing agents are present (e.g. winds). This cessation of entrainment and mixing was already noted by Ellison and Turner [1959] after a series of laboratory experiments. If the topography allows (i.e. the free horizontal length-scale of the flow is larger than the internal radius of deformation) the intrusion will be turned to the right by the rotation of the earth and eventually follow the right shore in a geostrophic balance [Gill, 1976; McClimans, 1978; Stern et al., 1982; Griffiths and Hopfinger, 1983; Wang, 1985; Asplin, 1994b]. Since the brackish layer is a surface phenomenon, the flow will be independent of changes in the bottom depth as long as the total depth is much larger than the depth of the intrusion (a reduced gravity model).

The results from two numerical simulations will be presented. One control simulation where the brackish layer is sufficiently resolved and one simulation with insufficient (low) vertical resolution (the LVR-simulation). The model domain consists of a 20 km wide and 38 km long bay with a river runoff at the inner right corner (looking out of the bay). Outside the bay is an open ocean. The bottom depth is 100 m except for the inner 5 km of the bay where the depth is 20 m. Bottom depth gradients are linear and do not exceed 1/100 (a changing bottom depth implies a tilting of the σ -surfaces). The freshwater volume flux is constant throughout the simulation ($Q = 200 \text{ m}^3/\text{s}$). Initially there are no motions or surface elevation, the salinity is 33 everywhere, and the temperature 10 °C. Because the problem is of a baroclinic nature, fine horizontal grid resolution is needed (to resolve the internal radius of deformation) and a grid size of 1 km is chosen. The parameter settings of the numerical model are as described in the previous section (for the wind-driven flow experiments) except for the internal and external time-steps, being respectively 300 s and 10 s (the CFL criterion is 11.28 s).

The two simulations to be discussed differ only by the vertical resolution. For the control simulation, with a total of 23 σ -levels, the upper 5 m has 11 σ -levels. This provides a fair resolution of the brackish layer even where the bottom depth is 100 m (Δz of 0.5 m and less). The LVR-simulation on the other hand, has 12 σ -levels. At 100 m depth it has a σ -level only each 2.5 m in the upper 10 m, being incapable of resolving the brackish layer properly. However, where the total depth is 20 m, even the LVR-simulation will (marginally) resolve this layer. Obviously, as the bottom depth (and hence the depths of the σ -levels) increases along the natural path of the brackish intrusion, the LVR-simulation will gradually fail to resolve it.

After 60 hours simulated the brackish intrusion has reached the outskirts of the bay, and Figure 4 shows a top view of current vectors (at every second horizontal grid node) and the isopycnals from the control simulation (left panel) and the LVR-simulation (right panel) in the upper σ -layer. The depth of the upper σ -layer is for the control simulation between 0.025 m and 0.125 m, and for the LVR-simulation between 0.125 m and 1.25 m. The results are as expected with a wider intrusion in the mixing zone near the river and an adoption of a geostrophic balance further seawards (the width of the intrusion scales as the internal radius of deformation). The results of the control simulation are also in excellent agreement with the results of a similar simulation but with a flat bottom of 20 m depth (not shown), indicating that bottom depth variations are unimportant for the dynamics of the brackish layer (as expected in these deep waters). Comparing the two results, the most pronounced differences are for the LVR-simulation that the flow makes a larger turn to the left in the inner part of

the bay before adopting a geostrophic balance in the outer part, and that the surface density is higher (note the reduced width of the outer part of the intrusion due to the smaller internal radius of deformation).

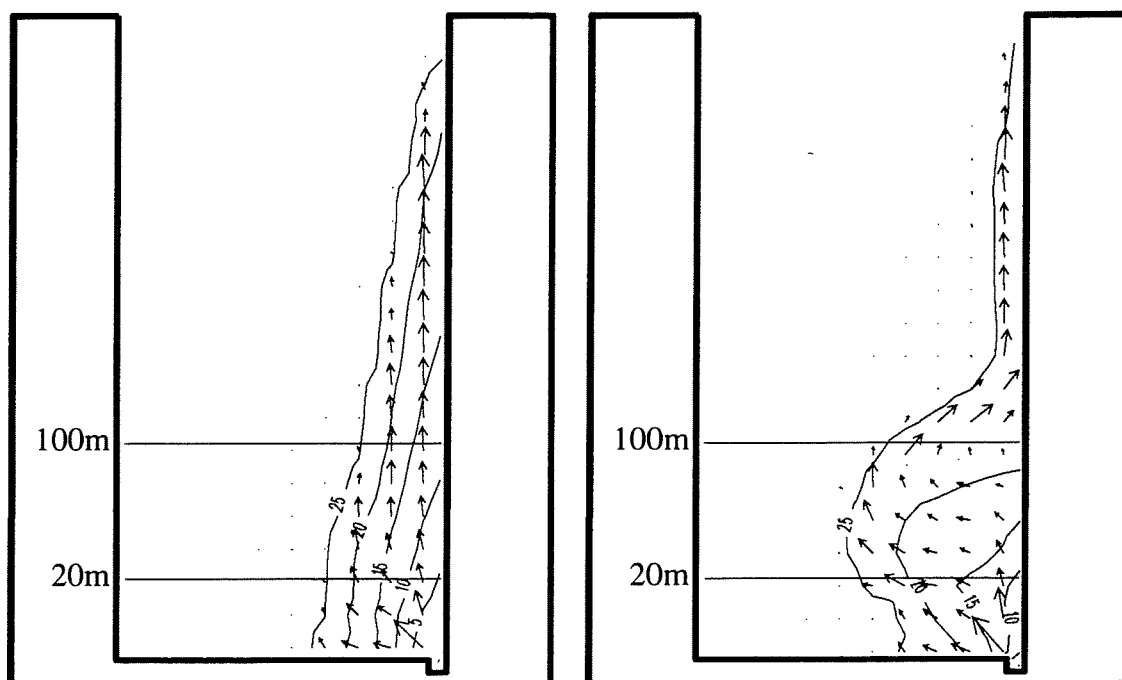


Figure 4. Top view of current vectors (only at each second grid node) and isopycnals from the control simulation (left panel) and the LVR-simulation (right panel) in the upper σ -level after 60 hours of constant runoff ($200 \text{ m}^3/\text{s}$) from the river at the bottom right corner of the bay. The bay is 20 km wide and 38 km long, and the bottom depth is as indicated 100 m in the outer part, 20 m in the inner part, and with a linear increase of depth between.

In Figure 5, vertical profiles of density (upper panel) and along-shore velocity (lower panel) in the upper 30 m and after 60 hours at the position 25 km from the river runoff and adjacent to the right shore are shown for both simulations. At this location the intrusions are geostrophically balanced. The depths where the values are calculated (i.e. mid-way between the depths of the σ -levels) are shown by circles (control simulation) and squares (LVR-simulation). The results of the control simulation are typical with strong vertical gradients in the upper 5 m and homogeneous conditions below, including a modest return flow. The sampling difficulties of the LVR-simulation results in a denser and deeper brackish layer. However, except for the upper metre, the two density profiles are not dramatically different. For the along-shore velocity though, the LVR-simulation overestimates the flow in the upper 10 m compared to the control simulation, and the return flow below 20 m is overestimated by more than 100%.

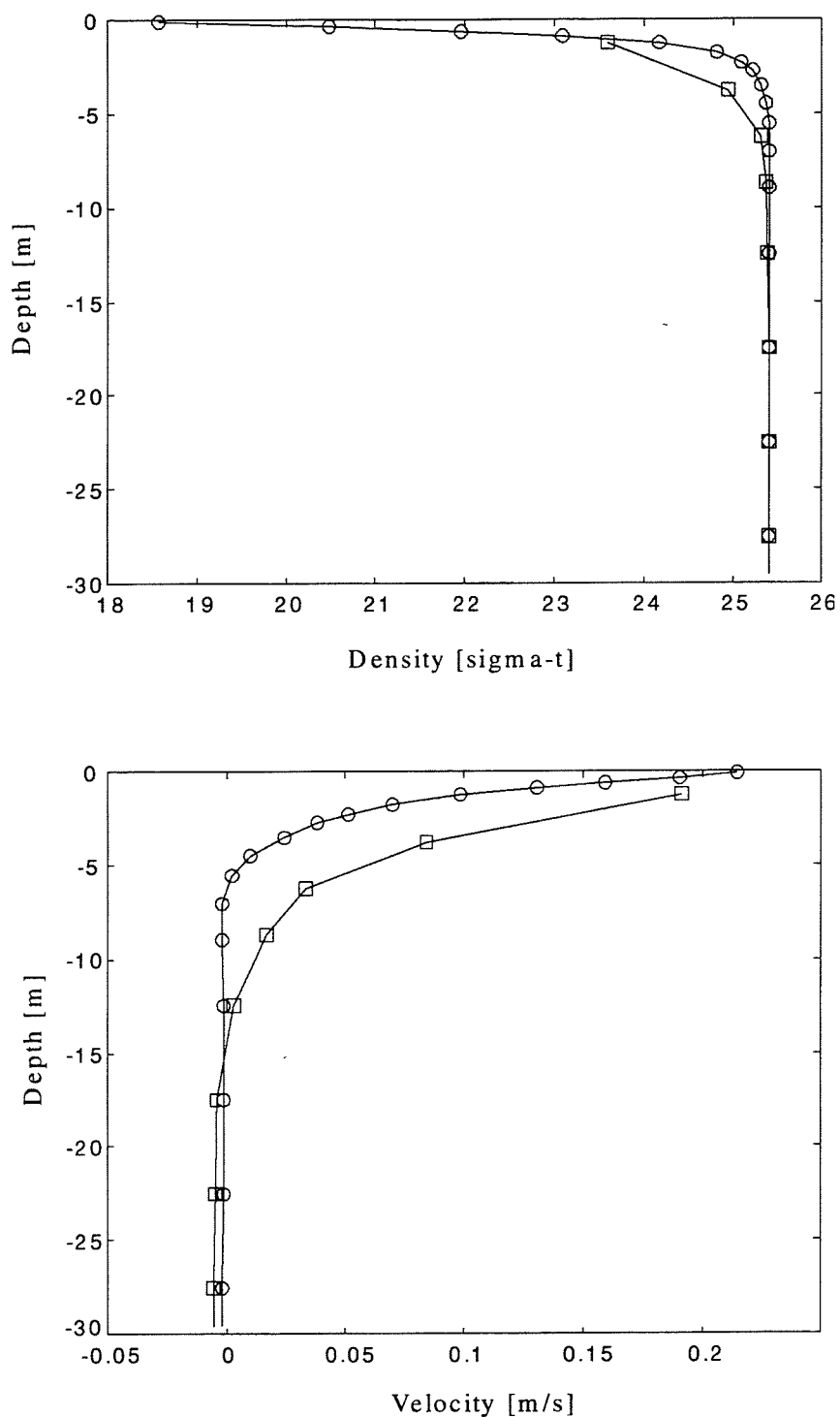


Figure 5. Vertical profiles of density (upper panel) and along-shore velocity (lower panel) after 60 hours at the position 25 km out the channel and adjacent to the right shore (i.e. where the brackish intrusion is in a geostrophic balance). The lines of the control simulation are marked by circles and the LVR-simulation by squares, with the markers representing the local depths of the σ -layers.

Volume flux vectors (depth-averaged flow) at each horizontal grid node are shown after 60 hours in Figure 6 for the control simulation (left panel) and the LVR-simulation (right panel). The volume flux of the control simulation is forming a cyclonic vortex in the inner part of the bay and a larger anticyclonic vortex further out. The maximum absolute value of the volume flux is approximately $400 \text{ m}^3/\text{s}$, and the net volume flux out of the bay is equal to the volume flux of the river runoff ($200 \text{ m}^3/\text{s}$). Qualitatively, the results of the LVR-simulation are not too different from the control simulation. However, quantitatively the LVR-simulation exceeds the control simulation by at least a factor of two with maximum absolute value of the volume flux being almost $1000 \text{ m}^3/\text{s}$. As for the control simulation, the net flux out of the bay equals that of the river runoff.

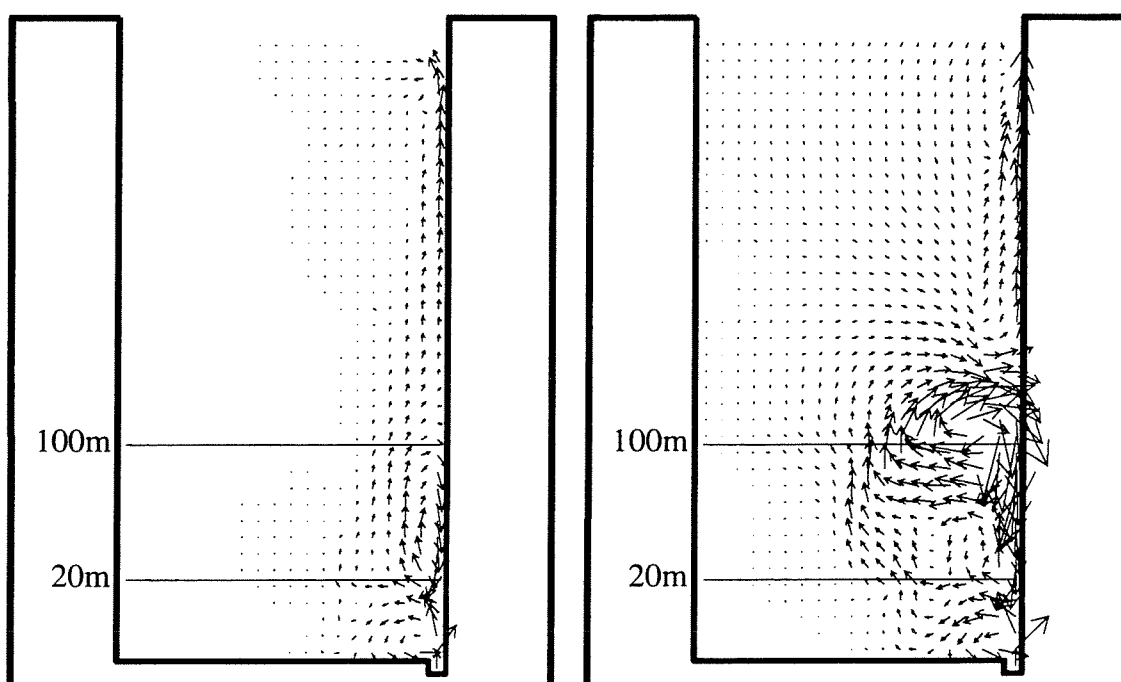


Figure 6. Top view of volume flux vectors for the control simulation (left panel) and the LVR-simulation (right panel) after 60 hours of constant runoff ($200 \text{ m}^3/\text{s}$) from the river at the bottom right corner of the bay.

To seek explanations for the deviating results of the LVR-simulation, it is quite obvious that the undersampling makes the brackish intrusion thicker with a greater volumetric flow. Then, mass balance requires more flow in the direction of the runoff, and there will be more mixing in the inner part of the bay. The mixing in the 20-100 m bottom slope zone will, to a large extent, be due to the gradual deterioration of the vertical resolution when the bottom depth increases. Such artificial mixing will introduce different baroclinic pressure gradients compared to the control simulation. This pressure field in combination with the need for a greater mass compensation flow towards the mixing zone will force the brackish-layer flow to make the large detour to the left. Another mechanism to enhance the anticyclonic vortex

in the inner part of the bay may be due to conservation of potential vorticity. An expression for this property can be derived from the primitive equations of the numerical model, with the viscous terms assumed negligible and a buoyancy sink term added. The buoyancy sink term will represent the effect of the inadequate vertical resolution. Generation of anticyclonic vorticity in the brackish layer is a possible solution for conservation of potential vorticity when buoyancy is removed. An analogue to this is conservation of angular momentum for a rigid body. This property is the product of the angular velocity (rotation) and the moment of inertia. If the moment of inertia is increased (e.g. by increasing the mass) the angular velocity must decrease.

5. Summary and Conclusions

From a number of numerical simulations with a σ -coordinate coastal ocean model, the effects of insufficient vertical resolution are examined. Two typical scenarios were chosen: Wind-driven homogeneous-water flow, and brackish-layer flow due to river runoff. Both scenarios have their typical vertical dynamics with strong sub-surface gradients. In a comparison study, several numerical simulations differing only by the vertical grid resolution were performed.

The simulations of wind-driven flow showed that the volume fluxes were reasonably calculated by all the simulations. This is most likely due to the robust result of Ekman [1905] that the volume flux from wind-driven flow is independent of the vertical structure of horizontal velocity. When it comes to the vertical velocity profile, however, a very fine resolution in the upper 5 metre is needed to capture this completely as calculated by the numerical model (vertical grid size of $O(\text{cm})$). If the large gradient of these upper metres are not resolved by the grid, the energy will be aliased onto resolved wave-lengths. In the simulations this appears mostly as a modest velocity increase distributed over a larger depth. An exceptional situation arises if the vertical gradients is partly well resolved, as in simulation *vr4* with three σ -levels in the upper metre and otherwise poor vertical resolution. In these cases, the aliasing leads to an accumulation of energy in the area resolving the shorter wavelengths. For simulation *vr4* this resulted in an overestimation of the surface velocity (at 0.25 m depth) by more than 30%.

In the brackish-layer flow experiments, both kinetic and potential energy are involved, thus the level of complication is raised compared to the wind-driven homogeneous-water flow experiments. In addition to an aliasing of an unresolved vertical velocity profile (similar as for the wind-driven flow) mass (and potential energy) will be artificially added by aliasing of the density profile. An insufficient vertical resolution leads in this case to a much greater recirculation within the bay.

It is clear that the results of the simulation not resolving the brackish layer (the LVR-simulation) are erroneous when comparing to the control simulation, and also that the differences are significant. However, if only the results of the LVR-simulation existed, they could have been accepted as "reasonable", being qualitatively not too different from those of the control simulation. Especially in a more realistic and complicated scenery, with many simultaneous forcing mechanisms and dynamical features, the errors due to poor vertical

resolution will be hard to discover. Also taken into account is the fact that (still) existent in 3D primitive equation numerical models are many “tuneable” parameters that can highly affect mixing and energy levels, hence it is probably possible to adjust the results of the LVR-simulation in the direction of the control simulation.

This work has shown that aliasing due to inadequate vertical resolution introduces errors that certainly will be critical for all applications relying on the vertical velocity profile or the density structure (e.g. water quality models and biological models). Calculations of wind-driven volume fluxes do not depend on the same high sub-surface resolution as the calculation of the wind-driven surface velocity, although it is perhaps not a good idea to use a 3D model (or misuse it) in strictly 2D problems. Finally, an easy way to eliminate these problems with insufficient vertical resolution is to add vertical grid nodes.

Acknowledgments

The numerical simulations were made possible by support from the Norwegian Supercomputing Committee (TRU) through a grant of computing time. Thanks to Jarle Berntsen, Benoit Cushman-Roisin, Ingvild Jensrud, Nils Gunnar Kvamstø, Morten Skogen, and Harald Svendsen for the help.

References

- Asplin, L., Simulation of river runoff in a fjord with a three-dimensional numerical model, Report of the Geophysical Institute, University of Bergen. 109 pp, 1994a.
- Asplin, L., The influence of the earth's rotation on flows in fjords and coastal oceans, Thesis of the Geophysical Institute, University of Bergen. 113 pp, 1994b.
- Asplin, L., H. Svendsen, and B. Cushman-Roisin, Observations and numerical simulations of freshwater runoff from Målselva into Malangen, Report of the Geophysical Institute, University of Bergen, 54 pp, 1995.
- Blumberg, A. F., and G. L. Mellor, Diagnostic and prognostic numerical circulation studies of the South Atlantic Bight, *J. Geophys. Res.*, 88, 4579-4592, 1983.
- Blumberg, A. F., and G. L. Mellor, A description of a three-dimensional coastal ocean circulation model. In *Three-dimensional coastal ocean models*, edited by N. Heaps, pp. 1-16, American Geophysical Union, 1987.
- Chereskin, T. K., Direct evidence for an Ekman balance in the California Current, *J. Geophys. Res.*, 100, 18261-18269, 1995.
- Craig, P. D., and M. L. Banner, Modeling wave-enhanced turbulence in the ocean surface layer, *J. Phys. Oceanogr.*, 24, 2546-2559, 1994.
- Craig, P. D., Velocity profiles and surface roughness under braking waves, *J. Geophys. Res.*, 101, 1265-1277, 1996.
- Ekman, V. W., On the influence of the earth's rotation on ocean-currents, *Ark. Mat. Astr. och Fysik*, Band 2, No. 11, 1-52, 1905.
- Ellison, T. H., and J. S. Turner, Turbulent entrainment in stratified flows, *J. Fluid Mech*, 6, 423-448, 1959.

- Garvine, R. W., Physical features of the Connecticut River outflow during high discharge, *J. Geophys. Res.*, 79, 831-846, 1974.
- Garvine, R. W., The role of brackish plumes in open shelf waters, In *The role of freshwater outflow in coastal marine ecosystems*, edited by S. Skreslet, pp. 47-65, NATO ASI Series G, 7, Springer-Verlag, Berlin, 1986.
- Garvine, R. W., and J. D. Monk, Frontal structure of a river plume, *J. Geophys. Res.*, 79, 2251-2259, 1974.
- Gill, A. E., Adjustment under gravity in a rotating channel, *J. Fluid Mech.*, 77, 603-621, 1976.
- Gnanadesikan, A., and R. A. Weller, Structure and instability of the Ekman spiral in the presence of surface gravity waves, *J. Phys. Oceanogr.*, 25, 3148-3171, 1995.
- Griffiths, R. W., and E. J. Hopfinger, Gravity currents moving along a lateral boundary in a rotating fluid, *J. Fluid Mech.*, 134, 357-399, 1983.
- Kaartvedt, S., and H. Svendsen, Effect of freshwater discharge, intrusion of coastal water, and bathymetry on zooplankton distribution in a Norwegian fjord system, *J. Plankton Res.*, 17, 493-511, 1995.
- Krauss, W., Ekman drift in homogeneous water, *J. Geophys. Res.*, 98, 20187-20209, 1993.
- Lentz, S. J., The surface boundary layer in coastal upwelling regions, *J. Phys. Oceanogr.*, 22, 1517-1539, 1992.
- Martin, P. J., Simulation of the mixed layer at OWS November and Papa with several models, *J. Geophys. Res.*, 90, 903-916, 1985.
- Martinsen, E. A., and H. Engedahl, Implementation and testing of a lateral boundary scheme as an open boundary condition for a barotropic model, *Coastal Eng.*, 11, 603-637, 1987.
- McClimans, T. A., Fronts in fjords, *Geophys. Astrophys. Fluid Dynamics*, 11, 23-34, 1978.
- Mellor, G. L., User's Guide for a three-dimensional, primitive equation, numerical ocean model, Report of the Princeton University, 39 pp, 1996.
- Mellor, G. L., and T. Yamada, Development of a turbulence closure model for geophysical fluid problems, *Rev. Geophys. Space Phys.*, 20, 851-875, 1982.
- Melsom, A., Realistic near-surface momentum mixing in the Princeton Ocean Model, *Rep.* 41, Norwegian Meteorological Institute, 22 pp, 1996.
- Price, J. F., R. A. Weller, and R. Pinkel, Diurnal cycling: Observations and models of the upper ocean response to diurnal heating, cooling, and wind mixing, *J. Geophys. Res.*, 91, 8411-8427, 1986.
- Skyllingstad, E. D., and D. W. Denbo, An ocean large-eddy simulation of Langmuir circulations and convection in the surface mixed layer, *J. Geophys. Res.*, 100, 8501-8522, 1995.
- Smagorinsky, J., General circulation experiments with primitive equations, I. The basic experiment, *Mon. Weather Rev.*, 91, 99-164, 1963.
- Stacey, M. W., S. Pond, and P. H. LeBlond, A wind-forced Ekman spiral as a good statistical fit to low-frequency currents in a coastal strait, *Science*, 233, 470-472, 1986.
- Stern, M. E., J. A. Whitehead, and B-L. Hua, The intrusion of a density current along the coast of a rotating fluid, *J. Fluid Mech.*, vol. 123, 237-265, 1982.
- Stigebrandt, A., A model for the seasonal pycnocline in rotating systems with application to the Baltic proper, *J. Phys. Oceanogr.*, 15, 1392-1404, 1985.

- Sweby, P. K., High resolution schemes using flux limiters for hyperbolic conservation laws. *SIAM J. Numer. Anal.*, 21, 995-1011, 1984.
- Treguier, A. M., J. K. Dukowicz, and K. Bryan, Properties of nonuniform grids used in ocean general circulation models, *J. Geophys. Res.*, 101, 20877-20881, 1996.
- Wang, D-P., Numerical study of gravity currents in a channel, *J. Phys. Oceanogr.*, 15, 299-305, 1985.
- Weller, R. A., and A. J. Plueddemann, Observations of the vertical structure of the oceanic boundary layer, *J. Geophys. Res.*, 101, 8789-8806, 1996.